ARCHIVES
of
FOUNDRY ENGINEERING

ISSN (2299-2944)
Volume 2026
Issue 3/2026

174 – 185

10.24425/afe.2026.158031

20/3

Published quarterly as the organ of the Foundry Commission of the Polish Academy of Sciences

Effect of Titanium Addition on Microstructure and Properties of Nitrogen-Alloyed High Chromium Cast Iron

B. Tokarski *, J. Jezierski, M. Janczak
Silesian University of Technology, Department of Foundry Engineering,
Towarowa 7, 44-100, Gliwice, Poland
Hydro-Vacuum S.A., Poland
* Corresponding author. E-mail address: b.tokarski@hv.pl

Received 30.06.2026; accepted in revised form 29.09.2026; available online 30.10.2026

Abstract

This paper investigates the effect of titanium alloying on the eutectic transformation of high-chromium cast iron (HCCI) containing a significant amount of nitrogen (2.4% C, 30% Cr, 0.1% N). The study was conducted under industrial conditions in a Polish foundry, with titanium added to liquid HCCI as ferroalloy. Maximum Ti concentrations did not exceed 1.5%. The influence of titanium was assessed via characteristic points on crystallization curves recorded by thermal analysis, compared to the equilibrium phase diagram modeled by Thermo-Calc software. Microstructure was examined by XRD and SEM-EDS, revealing TiN precipitation. Abrasion resistance was evaluated using the Miller test. Titanium addition slightly lowered the eutectic transformation temperature and shifted crystallization from eutectic to hypereutectic of HCCI and reduced cumulative mass loss by 35% in the Miller abrasion test.

Keywords: High chromium cast iron, TiN, Grain refinement, Abrasion resistance, Inoculation

1. Introduction

High-chromium white cast irons (HCCI) are widely used in applications involving severe abrasive and erosive–corrosive wear, including the mining, cement, paper and pump industries, where they are employed for handling fluids contaminated with solid particles [1,2]. Their high abrasion resistance results from the presence of hard carbides, most commonly of the M_7C_3 type, embedded in a ferritic, austenitic or martensitic metallic matrix. The morphology, size and volume fraction of the carbides are governed mainly by the chemical composition of the alloy and by the solidification conditions, whereas subsequent heat treatment primarily modifies the matrix and the secondary carbides. Depending on the carbon and chromium contents, hypoeutectic, eutectic or hypereutectic HCCI can be produced. Hypoeutectic grades, in which primary dendrites of the metallic phase are surrounded by the eutectic, offer the highest toughness but a relatively low carbide volume fraction [ref.]. Hypereutectic grades provide the highest abrasion resistance; however, coarse primary M_7C_3 carbides result in low impact toughness and high susceptibility to cracking, which leads to high casting rejection rates. Eutectic grades exhibit the most favourable casting characteristics, but in the as-cast state their abrasion resistance is lower than that of hypereutectic grades. A key objective in the development of these materials is therefore to combine the good castability of (near-)eutectic alloys with high wear resistance by controlling the size and morphology of the carbide phase.

© The Author(s) 2026. Open Access. This article is licensed under a Creative Commons Attribution 4.0 International License (http://creativecommons.org/licenses/by/4.0/), which permits use, sharing, adaptation, distribution and reproduction in any medium or format, as long as you give appropriate credit to the original author(s) and the source, provide a link to the Creative Commons licence, and indicate if changes were made.

Among HCCI, alloys containing approximately 30 wt.% Cr with a ferritic matrix are of particular importance for erosive–corrosive service, e.g. in slurry pumps handling corrosive media [ref.]. The high chromium content of the matrix ensures corrosion resistance, but a ferritic matrix cannot be strengthened by quench hardening. Consequently, in this group of alloys, refinement of the carbide phase during solidification is practically the only route to improving both toughness and wear resistance.

The most widely investigated approach to carbide refinement is alloying with strong carbide-forming elements, in particular titanium. Owing to its high affinity for carbon, Ti readily forms TiC in the melt; this phase precipitates prior to the chromium carbides and acts as a heterogeneous nucleation site for M_7C_3, effectively reducing the size of the carbide phase [2–5,14,15,22]. In hypereutectic irons, Ti-bearing particles act as nuclei of primary M_7C_3, which becomes finer and more isometric [2,4,5,15, 16,17,22]. Besides refining the carbides, Ti also modifies the solidification path. Because Ti-rich particles form in the liquid before the metallic and carbide phases, they bind part of the carbon (and nitrogen), lowering its effective content in the melt, while simultaneously providing substrates for the nucleation of the primary phases. Consequently, Ti additions change the characteristic temperatures recorded by thermal analysis and may change the type of the primary phase. In a near-eutectic chromium cast iron, Studnicki et al. [1] observed that the interval between the liquidus and the eutectic temperature widened from 0 to 24 °C after the addition of 2.29 wt.% Ti, i.e. the alloy no longer solidified as a eutectic one, and changes in primary crystallization were also reported for chromium cast irons inoculated with Ti and other elements [12,13].

TiC, TiN and their solid solution Ti(C,N) are interstitial compounds with the cubic NaCl-type (B1, Fm-3m) crystal structure, in which C and N atoms occupy the octahedral interstices of the fcc Ti sublattice and can substitute for each other over the whole composition range [20]. The lattice parameter of Ti(C,N) varies continuously, in accordance with Vegard's law, from about 0.433 nm for TiC to about 0.424 nm for TiN. The melting points are about 3067 °C and 2950 °C, the Vickers hardness is approximately 28–35 GPa for TiC and 18–21 GPa for TiN, and the densities (≈4.91 and ≈5.4 g/cm³, respectively) are much lower than that of liquid cast iron (≈7 g/cm³) [20]. Owing to the higher affinity of Ti for N, TiN is thermodynamically more stable than TiC and precipitates first; in Ti- and N-bearing melts, the particles have been reported to consist of an N-rich core covered by a C-richer Ti(C,N) layer [8,22]. The particles are typically faceted (cubic or polyhedral), which, together with their low density, favours their flotation and clustering in the melt; at excessive Ti contents this leads to agglomeration of Ti-rich particles and to casting defects [3].

Nitrogen itself is an active alloying element in HCCI. In the absence of strong nitride formers, it dissolves in the metallic matrix and in the M_7C_3 carbides, increases the number of carbide nuclei and refines the eutectic and primary carbides [10,18]. In the presence of Ti, nitrogen is bound into TiN [6,7] and Ti(C,N), and the simultaneous addition of both elements has proven particularly promising [8,10,11]. Ding et al. 8 showed that increasing the N content from 0.028 to 0.075 wt.% in a Ti-containing HCCI produced finely dispersed Ti(C,N) particles and refined the M_7C_3 carbides. Like TiC, TiN satisfies Bramfitt's criteria for heterogeneous nucleation of M_7C_3 9, and the crystallographic misfit between Ti(C,N) and M_7C_3 remains below 10% over the whole Ti(C,N) composition range, indicating that these particles can act as efficient nucleation substrates [8,9].

The conditions of Ti(C,N) formation in HCCI are, however, strongly affected by the chromium content. Chromium increases the activity of titanium (e_Ti^Cr > 0) but decreases the activity of nitrogen, i.e. increases its solubility (e_N^Cr < 0) [6,7]. It strongly increases the critical solubility of nitrogen and decreases the solubility of titanium in TiN-saturated Fe–Cr melts [7,19]. Since these effects act in opposite directions with respect to TiN precipitation, their net result depends on the Ti and N contents, and the conditions of Ti(C,N) formation in 30 wt.% Cr cast irons differ from those in low-alloyed iron melts. Therefore, the effects of Ti in nitrogen-containing HCCI cannot be separated from the effects of nitrogen.

Despite the increasing number of publications dealing with the titanium-assisted modification of HCCI, there is still a shortage of systematic studies focused specifically on ferritic, nitrogen-containing alloys with high chromium content (~30 wt.% Cr), and on a quantitative characterization of their slurry wear. The Miller test, standardized in ASTM G75, consists of subjecting block-shaped specimens to an oscillatory motion in an abrasive slurry and determining the Slurry Abrasion Response (SAR) number, a parameter directly relevant for pump sleeves, pipe bends and other components operating in mineral processing environments. The aim of the present study is therefore to determine how titanium additions, in combination with nitrogen, modify the solidification behaviour recorded by thermal and derivative analysis (TDA), the morphology of the carbide phase, the impact toughness and the slurry wear resistance of ferritic ~30 wt.% Cr cast iron.

2. Methods

Under industrial foundry conditions, the base high-chromium cast iron was melted in a 500 kg, 270 kW induction furnace. Titanium was then added in the form of a FeTi70 ferroalloy so that the final Ti content in the liquid alloy reached approximately 1.0 and 1.5 wt.% (1.07 and 1.56 wt.% analysed, Table 1). After the addition of the alloying element, the melt was superheated to 1600 °C and held for 3–5 min, and then cooled down to the pouring temperature of 1580 °C. The chemical composition of the obtained cast iron is shown in Table 1. At each tap from the furnace into the ladle, the cast iron was deoxidized by an Al addition.

During the experiment, test material was cast in the form of ϕ30 × 400 mm bars, impact test specimens, samples for abrasion testing using the Miller test, and small discs for chemical composition determination. Microstructural characterization was carried out on specimens cut from the Ø30 × 400 mm bars using a Zeiss AxioObserver Z1m light microscope, X-ray diffraction (XRD) with an Empyrean PixCel³D diffractometer, and a FEI SCIOS scanning electron microscope equipped with an EDAX TEAM v.4.4 EDS X-ray microanalyzer.

Carbon content in the alloy was determined using a Leco CS600 analyzer, whereas the remaining alloying elements were measured by the OES method with a Metek SpectroMaXx4 Crystallization data were recorded using a SIMEX CMC99 recorder and a standard thermal analysis cup (Heraeus

Electro-Nite) with a type K thermocouple; the data acquisition frequency was set to 1 s. The characteristic temperatures (T_L, $T_{E,min}$, T_E, T_{sol}) were determined from the local extrema and inflection points of the first derivative of the cooling curve.

Metallographic specimens were cut from the Ø30 × 400 mm bars at a distance of 200 mm from the bar end and at mid-radius, hot-mounted in conductive resin, ground on SiC papers from P120 to P2000 and polished with 3 and 1 µm diamond suspensions, followed by 0.05 µm colloidal silica. The microstructure was revealed by etching with aqua regia; SEM-BSE observations and EDS analyses were performed on unetched / etched – confirm specimens. Light micrographs were taken at magnifications of 200×, 500×. Phase segmentation was performed using the Trainable Weka Segmentation algorithm (Fiji/ImageJ) based on a Fast Random Forest classifier; the classifier was trained on representative regions of M_7C_3 carbides, Ti(C,N) particles and the metallic matrix, and then applied uniformly to all specimens micrographs.

XRD measurements were performed for all three alloys under identical conditions using Cu Kα radiation (λ = 0.15406 nm), 40 kV/40 mA, a 2θ range of 20–120°, a step size of 0.013° and step time of 300s. SEM observations were carried out in secondary-electron (SE) and backscattered-electron (BSE) modes; BSE images were acquired with a concentric backscatter (CBS) detector at an accelerating voltage of 20 kV, a beam current of 3.2 nA, a working distance of 6.7–8.3 mm and at various magnifications of 200 to 2000x. The EDS results for N and C were treated as qualitative only.

Microhardness of the metallic matrix and the M_7C_3 carbides was measured with a Anton Paar platform under a load of 0.098 N (HV0.01) with a dwell time of 15s. Three indentations (n = 3) were made in each phase of each alloy; indentations in carbides were accepted only if the whole imprint lay inside a single carbide.

Unnotched Charpy specimens 10 × 10 × 55 mm were tested. The tests were carried out at room temperature (22 ± 2 °C) on a VEB 402/30 pendulum impact tester with a nominal work of 5 kpm results were recalculated in accordance with ISO 148-1, the absence of the notch is common practice for brittle white cast irons. Three specimens were tested per alloy.

Abrasive wear was evaluated using a Miller test apparatus in accordance with ASTM G75, employing a SiC–water mixture with a 1:2 ratio as the abrasive medium. Two specimens of were tested per alloy under a load of 22.24 N; the mass loss was measured with an accuracy of 0.1 mg after each 4 h interval up to a total test time of 16 h, and the SAR number was calculated according to ASTM G75.

All results are reported as mean ± standard deviation (SD), with the number of measurements n given in the tables. Differences between the alloys were evaluated by one-way ANOVA followed by Tukey's HSD post-hoc test (α = 0.05) or Welch's test for unequal variances. For the microhardness (n = 3), Miller (n = 2) and Charpy (n = 3) tests, the statistical power is limited, and the corresponding comparisons are treated as indicative.

Table 1.
Chemical composition of High Chromium Cast Iron in wt. %

Heat	C	Si	Mn	Mo	Ni	Cr	Ti	N
Base Iron	2.45	1.64	0.38	0.089	0.297	30.03	0.0079	0.11
Ti4	2.41	2.01	0.4	0.067	0.27	29.79	1.07	0.149
Ti8	2.41	1.93	0.412	0.1	0.3	29.79	1.56	0.11

3. Results

Figure 1 shows the pseudo-binary Fe–Cr–C phase diagram calculated for 30 wt.% Cr and 2 wt.% C using Thermo-Calc in order to gain insight into the crystallization process; the composition range of the investigated alloys is marked. The diagram is used only as a qualitative framework, because it does not include Si, Mn, N and Ti. The eutectic point for the assumed alloy composition was read at 1288 °C and 2.66 wt.% C. For carbon content below 1.8 wt.%, such an alloy solidifies as fully ferritic cast iron without an austenite transformation, which eliminates the possibility of hardening and strengthening this cast iron by conventional heat treatment. This agrees with experimental studies of 30 wt.% Cr cast irons, in which a ferritic matrix with eutectic M_7C_3 carbides was observed [21], and with the XRD and SEM results of the present study (Figs. 3,xxx). Within the composition range given in Table 1, the base cast iron is expected to crystallize slighty hypoeutectically, as δ-ferrite dendrites followed by the δ + $M_{23}C_6$ + M_7C_3 eutectic; the $M_{23}C_6$ carbides predicted by the calculation at lower temperatures were not detected by XRD (Fig. 3), which indicates that the M_7C_3 → $M_{23}C_6$ transformation was suppressed at the cooling rate of the castings. To verify the crystallization process during industrial melting, a sample was poured for thermal-derivative analysis (TDA); the cooling curve and its first derivative are shown in Fig. 2, and the characteristic temperatures are listed in Table 2. Analysis of the curve indicates that the cast iron is near-eutectic, with an eutectic transformation temperature T_E at 1280.8°C and carbon content of 2.45 wt.%. The difference between the calculated eutectic composition and the near-eutectic behaviour of the base iron is consistent with the effect of elements not included in the calculation, mainly Si (1.6–2.0 wt.%) and N and with the non-equilibrium solidification of the industrial casting.

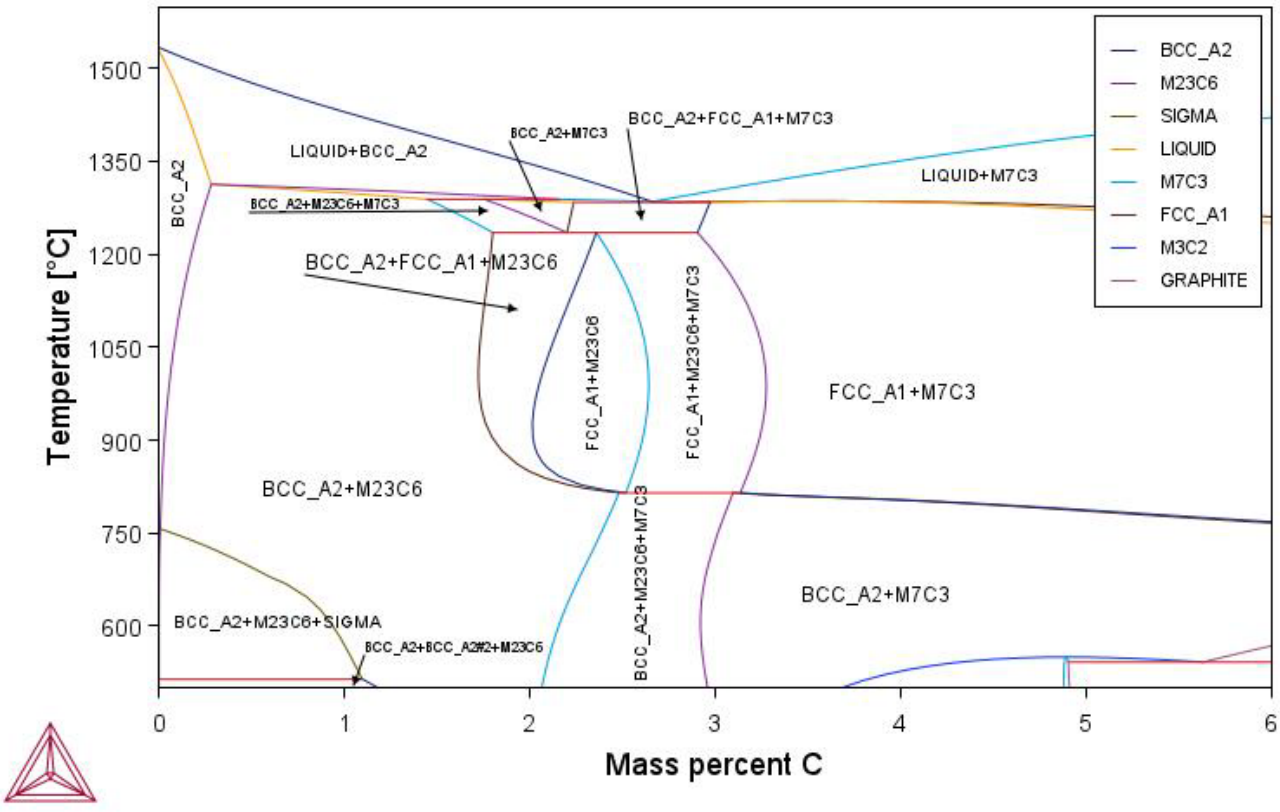


Fig. 1. Pseudobinary phase diagram of Fe-C

Table. 2
Characterisitc temperatures determined form the cooling curves (Figs.2 and 5)

	T_L	T_E	Type
Base Iron	-	1280.8	near-eutectic
Ti4	-	1276.8	near-eutectic
Ti8	1280.3	1272.2	hypereutectic

The XRD pattern of the base cast iron (Fig. 3) revealed several dominant peaks assigned to a BCC crystal lattice, marked with a green dashed line, and reflections of M_7C_3, indicating that the metallic matrix consists of a chromium-alloyed ferrite and a network of M_7C_3 carbides. No reflections of austenite or $M_{23}C_6$ were detected. The fully ferritic character of the matrix is supported by the SEM-BSE images taken at 1000x, in which the matrix of all three alloys shows only grain-orientation contrast, without martensite laths or retained austenite. In the base cast iron, M_7C_3 carbides exhibit an elongated, acicular morphology. Using image analysis in the Fiji/ImageJ software, the total area fraction of the carbide phase was determined as 20.6%; the SEM microstructure of the base iron and Ti alloyed is shown in Fig. 4.

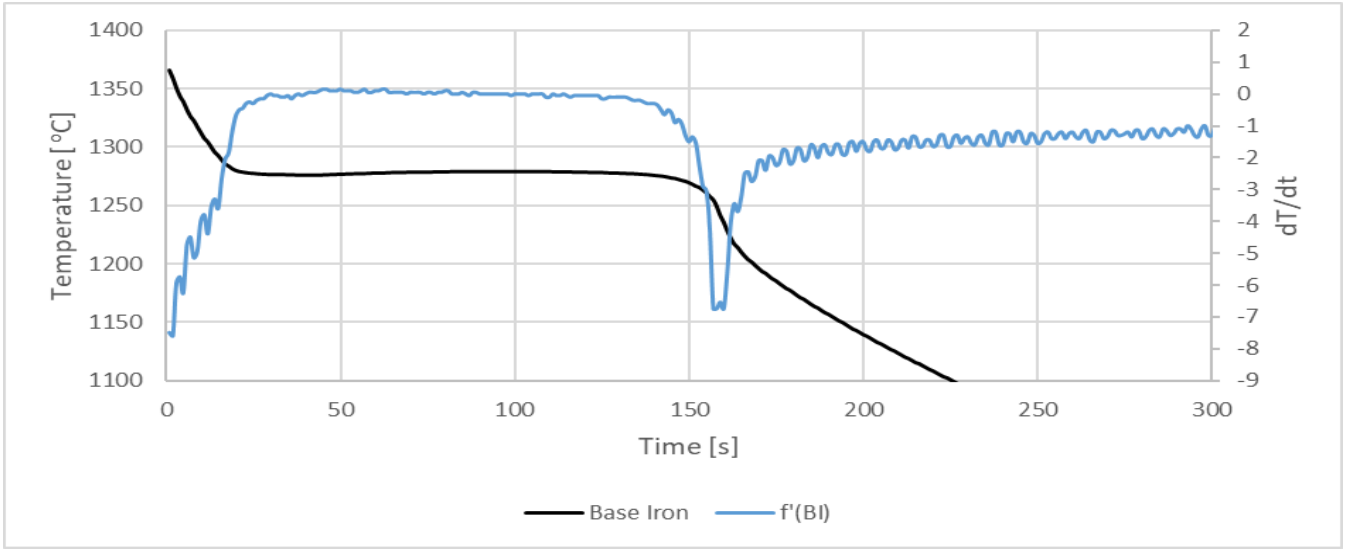


Fig. 2. Cooling curve of base iron

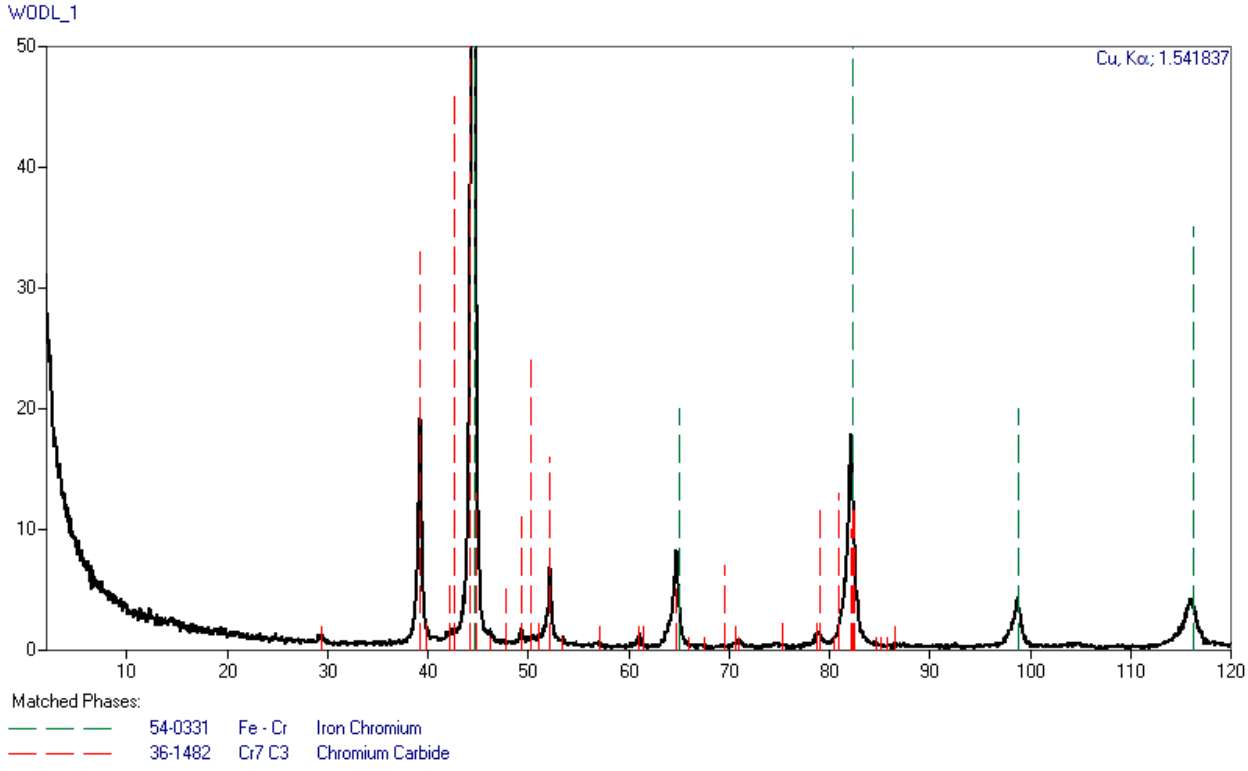


Fig. 3. XRD diffractogram of base iron

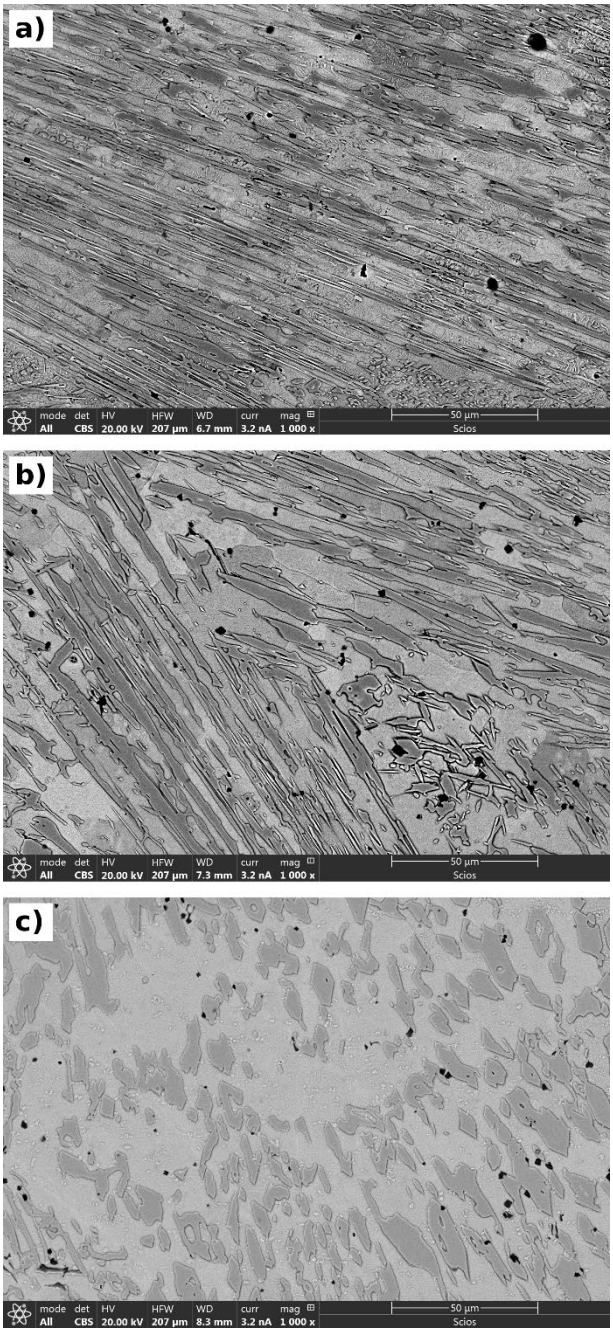


Fig. 4. SEM-BSE micrographs (CBS detector, 20 kV, 1000x) of Base Iron (a), Ti4 (b) and Ti8 (c): ferritic matrix (light grey), M_7C_3 carbides (dark grey) and Ti(C,N) particles (black, faceted)

The crystallization curves for the Ti4 and Ti8 cast iron are shown in Fig. 5. From these curves it can be seen that a Ti addition of about 1 wt.% (Ti4, 1.07 wt.% Ti) practically does not change the crystallization character and the alloy remains near-eutectic, whereas a significant change in the crystallization mode occurs for the Ti8 alloy containing 1.56 wt.% Ti, which solidifies as a hypereutectic cast iron with a liquidus temperature T_L=1280.3°C related to the precipitation of primary M_7C_3. The Ti addition slightly reduced the eutectic transformation temperature to 1276.8 °C in Ti4 and to 1272.2 °C in Ti8 (Table 2).

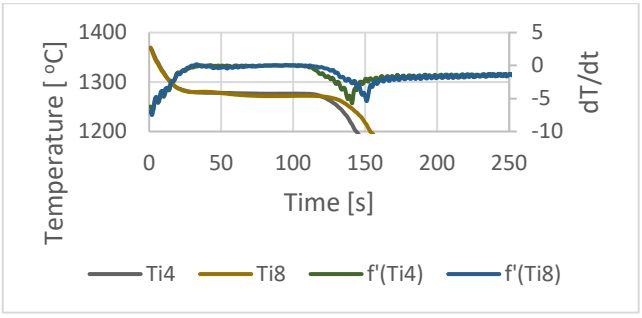


Fig. 5. Cooling curves of Ti4 and Ti8 high chromium iron

With increasing Ti content, the morphology of the carbide phase changes from needle-like to regular hexagonal particles, typical of primary M_7C_3 rods sectioned perpendicular to their axis. The area fraction of the carbide phase increased to 27.9 and 29.7 in Ti4 and Ti8, respectively. Representative micrographs of the metallographic cross-sections are shown in Fig. 4, the carbides still form eutectic colonies of long parallel laths, locally accompanied by regions of finer branched carbides, whereas in Ti8 (Fig. 4c) the carbides are compact, isometric or polygonal, some of them with hollow cores, which is typical of primary M_7C_3 rods sectioned perpendicular to their axis. A comparison of the carbide and Ti(C,N) area fractions in the investigated cast iron is summarized in Table 3.

Table 3.
Phase area fraction

	Carbide area [%]	TiN area [%]
Base Iron	20.6 ± 3.6	0
Ti4	27.9 ± 5.2	3.071 ± 1.2
Ti8	29.7 ± 5.4	2.601 ± 1.1

In the metallic matrix and within the M_7C_3 carbides of the Ti-modified samples, fine faceted precipitates were observed which, based on SEM-EDS analysis, were identified as Ti-rich particles containing N and C, as shown by the element distribution maps in Fig. 7 for Ti4 and Fig. 8 for Ti8 and by the EDS line scans in Fig. 13. In the BSE images (Fig. 4b,c), these particles appear as black, sharply faceted (square to polygonal) particles about 1–3 µm in size, dispersed in the ferrite, at the carbide/matrix interfaces and occasionally inside the carbides; their dark contrast results from their lower mean atomic number compared with the Cr-rich M_7C_3 carbides and the Fe-rich ferrite. Such faceted particles are absent in the Base Iron (Fig. 4a), in which only rounded dark features, most likely pores or oxide inclusions, are visible. SEM-EDS analysis also revealed a number of inclusions associated with deoxidation products formed due to the Al addition (Fig.7) frequently located in the centres of the Ti-rich particles. These precipitates form clusters and colonies which may influence the mechanical properties of the castiron, as reported previously by other authors [3,12,13]

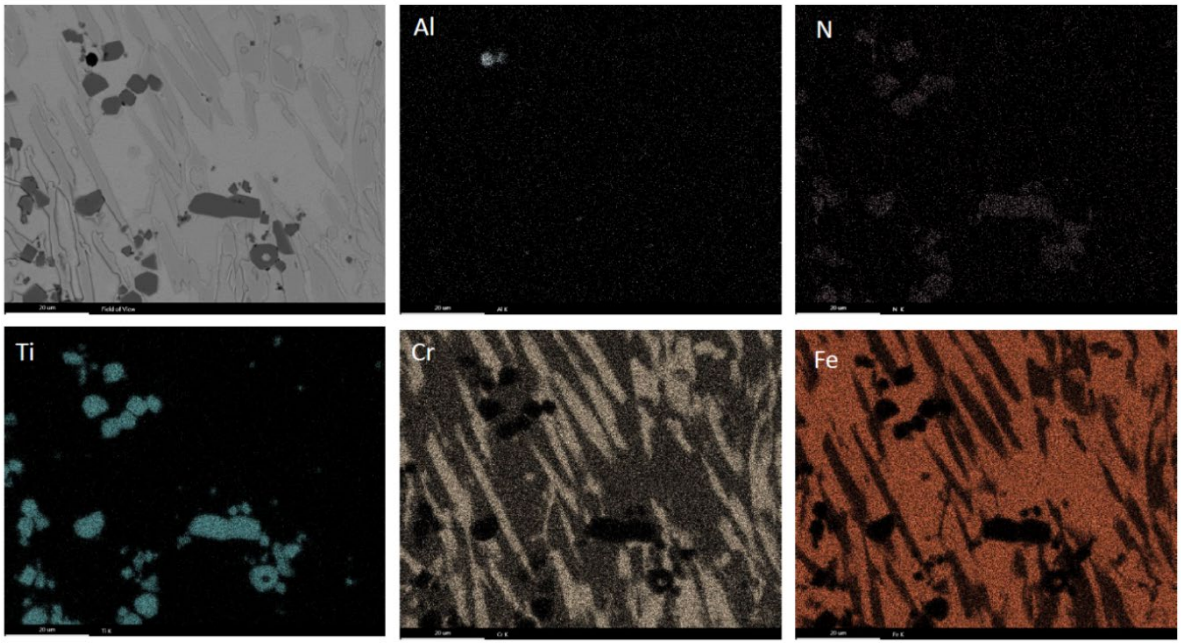


Fig. 7. SEM element distribution map of Ti4

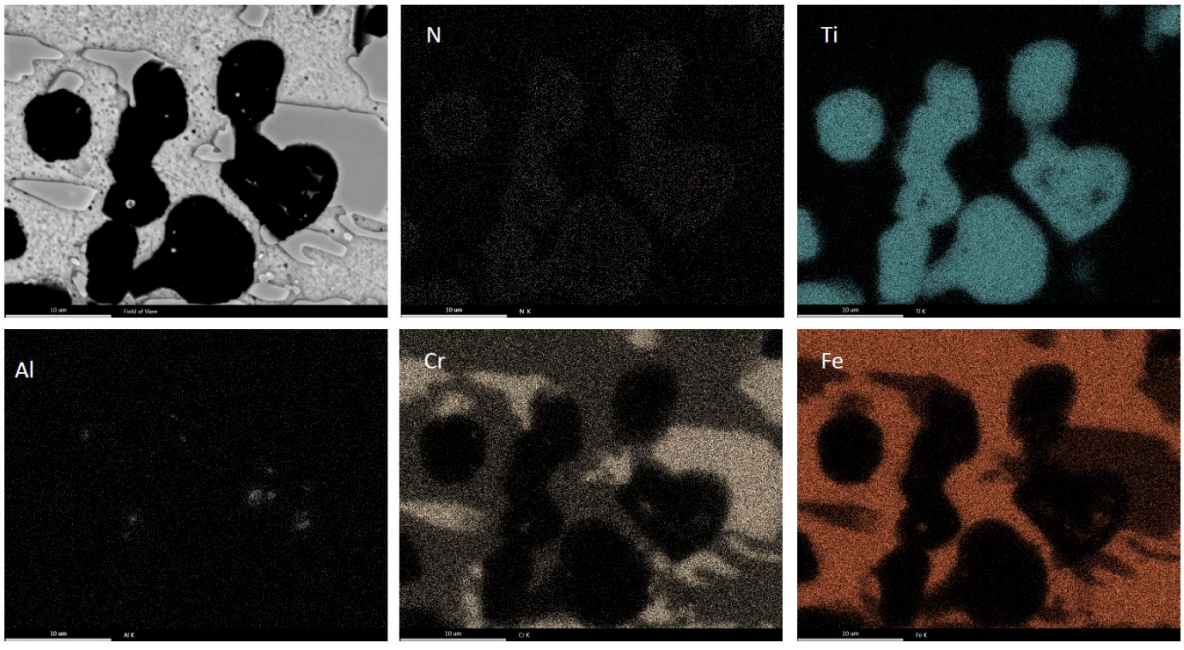


Fig. 8. SEM element distribution map of Ti8

An unequivocal distinction between TiN, TiC and intermediate Ti(C,N) compositions is not possible on the basis of the present data. The three phases are isostructural (NaCl type, Fm-3m) and their lattice parameters differ by only about 2% [20], so their reflections overlap in the XRD patterns, whereas in EDS the N Kα line overlaps with the Ti Ll line and carbon quantification is affected by contamination. Therefore, throughout this paper the Ti-rich particles are designated Ti(C,N), i.e. titanium carbonitride of an unspecified C/N ratio.

The XRD patterns of the Base Iron (Fig. 3), Ti8 (Fig. 9a) and Ti4 (Fig. 9b) are dominated by the reflections of the Cr-alloyed ferrite (bcc, indexed as $Cr_{0.1}Fe_{0.9}$) at $2\theta \approx 44.6°$, 65.0°, 82.3° and 98.9°, accompanied by weak reflections of M_7C_3 (indexed as Cr_7C_3). No reflections of austenite or $M_{23}C_6$ were found in any of the alloys. In the Ti4 pattern, no separate reflections of a cubic Ti-

rich phase could be distinguished: the strongest Ti(C,N) reflections, (111) at $2\theta \approx 36–37°$ and (200) at $2\theta \approx 42–43°$ for Cu Kα radiation [20], either fall below the detection limit, which is expected for a phase occupying about 3% of the section area (Table 2), or overlap with the M_7C_3 reflections. Therefore, the presence of Ti(C,N) in Ti4 is documented by SEM-EDS (Fig. 10) rather than by XRD. In the Ti8 pattern, reflections initially assigned to TiC were detected.

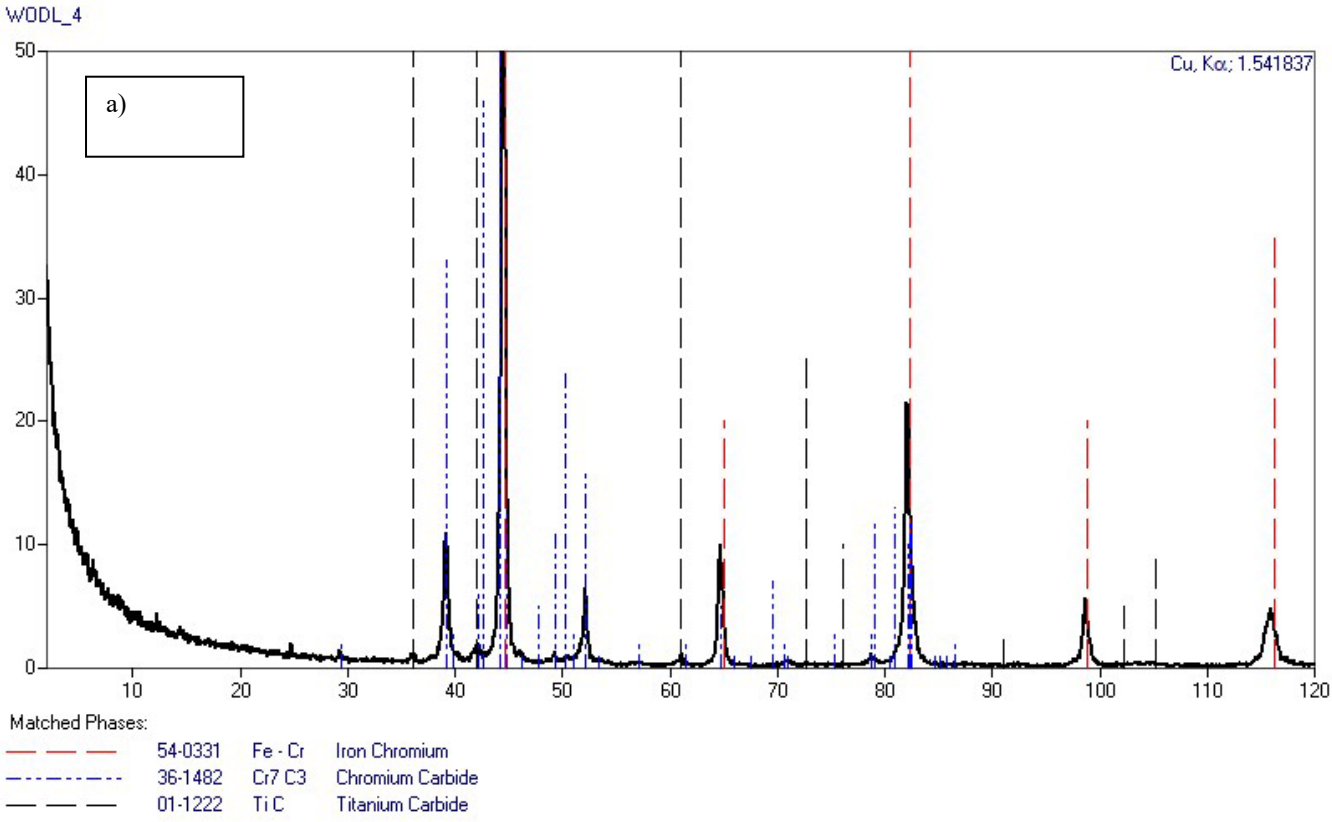
The role of nitrogen can be assessed from a simple mass balance. The stoichiometric Ti/N mass ratio in TiN is 3.42; thus, the nitrogen contained in Ti4 (0.149 wt.%) and Ti8 (0.11 wt.%) can bind at most about 0.51 and 0.38 wt.% Ti, respectively, i.e. less than half of the Ti introduced (1.07 and 1.56 wt.%). The remaining Ti (≈0.56 and ≈1.18 wt.%) must be present as C-rich Ti(C,N) or dissolved in the matrix and in M_7C_3, which independently supports the Ti(C,N) designation. If this excess Ti were entirely bound as TiC, it would consume up to about 0.141 wt.% C in Ti4 and 0.297 wt.% C in Ti8. The volume of stoichiometric TiN that could be formed from the available nitrogen in Ti4 (≈0,9% vol.%) is clearly smaller than the measured area fraction of Ti-rich particles (3.07%, Table 2), which again indicates that the particles contain a considerable amount of carbon and/or that the segmented area includes oxide inclusions. Notably, Ti4, containing more nitrogen, exhibits a higher area fraction of Ti(C,N) than Ti8 despite its lower Ti content. This suggests that nitrogen limits the amount of the early-formed N-rich Ti(C,N), and that part of the particles in Ti8 may have been lost by flotation and agglomeration, given their low density compared with the melt [3,20].

Nitrogen also controls the temperature at which Ti(C,N) forms. Using the equilibrium constant for the dissolution of TiN in liquid iron, $\log K = -15780/T + 5.63$ [6], the solubility product at the superheating temperature of 1600 °C (1873 K) is about 1.6×10^{-3} $(\text{mass\%})^2$, whereas the products [%Ti]·[%N] in Ti4 and Ti8 are 0.159 and 0.172, i.e. about two orders of magnitude higher. Chromium markedly increases the critical nitrogen solubility and decreases the Ti solubility in TiN-saturated Fe–Cr melts [7,19], so the actual supersaturation in the 30 wt.% Cr melt is lower than this simple estimate; nevertheless, a calculation including the interaction parameters for Fe–30Cr melts [7,19] indicates that N-rich Ti(C,N) is stable already in the liquid bath at 1600 °C, i.e. well above the liquidus temperature. This is consistent with the formation of Ti(C,N) during holding in the furnace and with the observed clustering. In the practically Ti-free base iron, nitrogen remains dissolved in the matrix and in M_7C_3, where it contributes to the refinement of the eutectic carbides and to the strengthening of the ferrite [10,18]. The addition of Ti transfers most of this nitrogen into Ti(C,N); hence, the effects attributed to Ti in the present study are in fact combined effects of Ti and N: nitrogen determines the amount and the formation temperature of the N-rich Ti(C,N) nuclei, while the Ti in excess of the N stoichiometry reacts with carbon.

With increasing Ti content in the alloy, a decrease in microhardness was observed for both the metallic matrix and the carbide phase compared to the base cast iron, which can be associated with partial depletion of the melt in carbon consumed for the formation of titanium carbonitride phases Ti(C,N). The measured microhardness shown in Table 3. The hardness of $(Cr,Fe)_7C_3$ depends on its Cr/Fe ratio and on the substitution of other elements [23]. In the base iron, part of the nitrogen may be dissolved in the carbides, whereas in the Ti-containing alloys nitrogen is bound in Ti(C,N). The ferrite hardness (344–382 HV0.01) is high owing to solid-solution strengthening by Cr, Si and interstitial N and C. Binding of N and C in Ti(C,N) reduces the interstitial content of the ferrite, which may explain the tendency towards lower matrix hardness despite the slightly higher Si content of the Ti-bearing heats

Table 4.
Microhardness of phases HV 0.01

Heat	Matrix	Carbides
Base Iron	382 ±32	1556 ±51
Ti4	373 ±24	1528 ±183
Ti8	344 ±33	1467 ±81



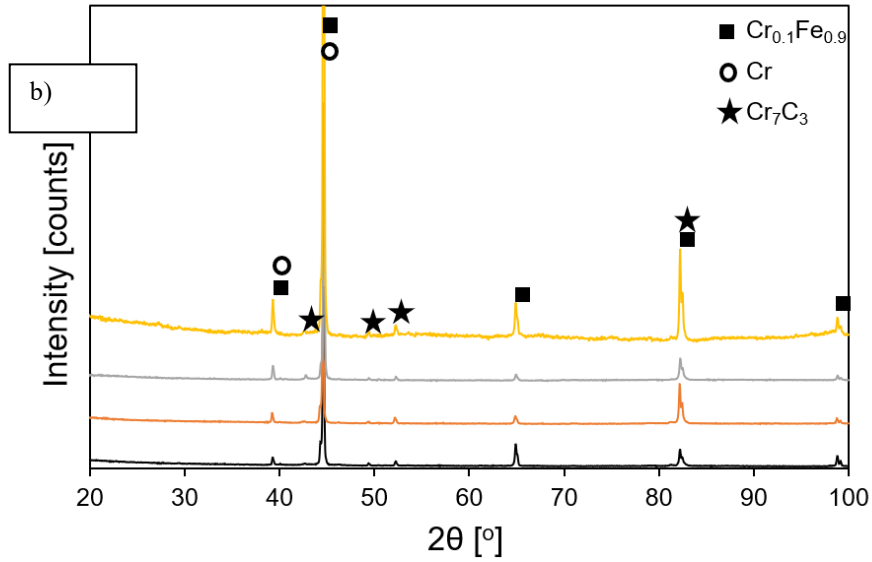


Fig. 9. XRD diffractogram of Ti alloyed High Chromium Cast Iron: a) Ti8 b) Ti4

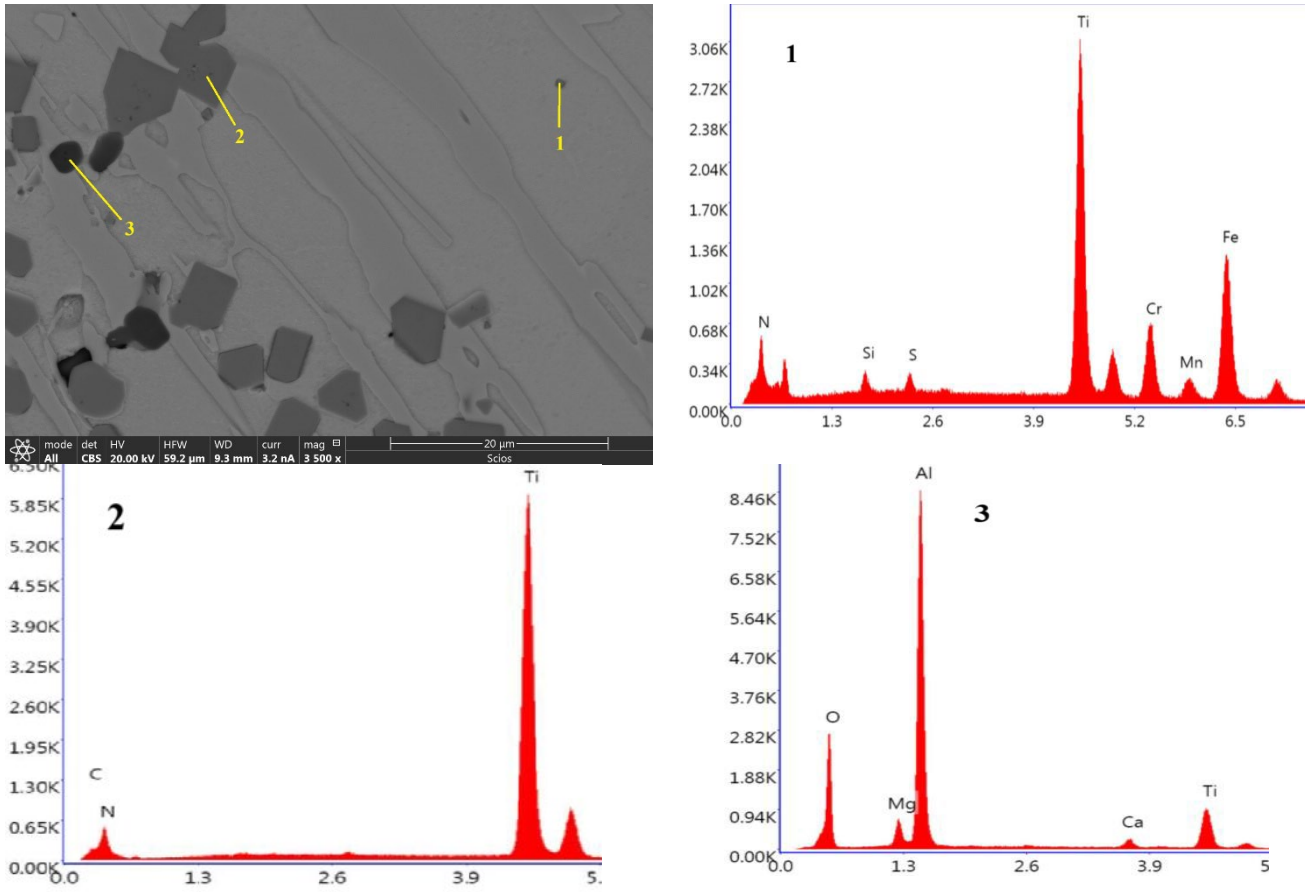


Fig. 10. SEM EDS praticle analysis of Ti4 iron

The cast iron modified with 1.5 wt.% Ti (Ti8) exhibited the lowest cumulative mass loss in the Miller abrasion test (ASTM G75) compared to the base cast iron and the Ti4 alloy. The results from two specimens of each tested alloy after 16h of load are presented in Fig. 10. On average, the Ti8 cast iron showed a cumulative mass loss lower by 227 mg than the base cast iron and by 178 mg compared to Ti4, which corresponds to a reduction in abrasive wear of 35% and 30%, respectively. The results obtained are reflected in the SAR values, which for the investigated alloys are 554 and 528 for the base iron and Ti4 respectively. The SAR number 347 was reached by Ti8. The improvement of wear resistance without any increase in the microhardness of the phases (Table 3) is only apparently inconsistent with the general rule that harder materials wear less. In two-phase white irons abraded by particles harder than the carbides, the wear rate is controlled not by the average hardness, but by the volume fraction, size, spacing and matrix support of the hard phases [23-26].

M. Dojka et al. [3-5] observed that, due to its physical properties, TiC forms clusters during crystallisation rather than being uniformly distributed within the structure. According to the authors, these TiC agglomerations could reduce the impact strength of the alloy. During the present study, it was observed that TiN, similarly to TiC, forms agglomerations as shown in Fig. 11. The impact toughness of the alloy was then tested using the Charpy method on unnotched samples. An analysis of the impact strength results shown in Table 5 reveals that, as the Ti content increases, the impact toughness of the alloy decrease by as much as 50%, reaching a value of 5.2 J/cm², whereas the base alloy had an impact toughness of 10.7 J/cm².

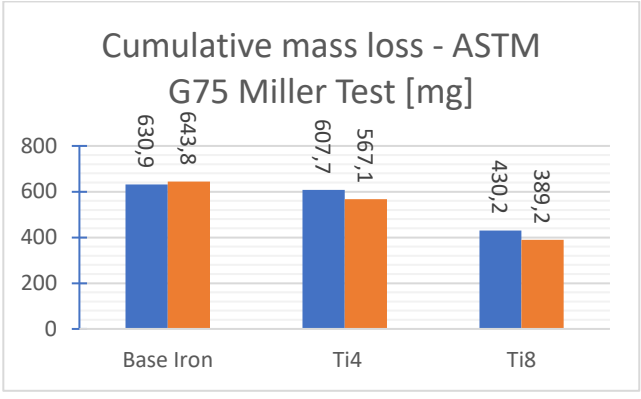


Fig. 11. Cumulative mass loss of tested High Chromium Cast iron

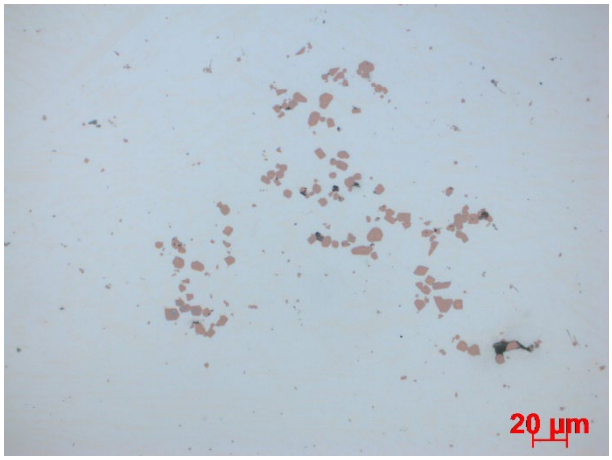


Fig. 12. TiN clusters in Ti4 high chromium cast iron, 500x

Table. 5.
Impact toughness of High Chromium Cast Iron, n=3

	KC [J/cm^2]
Base iron	10.7± 1.14
Ti4	8.25± 0.44
Ti8	5.2± 0.45

4. Conclusions

The study was performed on single industrial heats, so the Ti effect cannot be fully separated from the simultaneous differences in Si (1.64 vs 1.93–2.01 wt.%) and N (0.11–0.149 wt.%) contents. The thermodynamic calculations did not include Si, N and Ti, and the C/N ratio of the Ti-rich particles was estimated only indirectly. The number of specimens in the wear (n = 2) and impact (n = 3) tests was limited. The mechanisms discussed in Sections 3.2–3.5 should therefore be verified with additional heats with controlled Ti, N and Si contents, TEM/EBSD analysis of the Ti(C,N)–M_7C_3 interfaces and multicomponent thermodynamic calculations.

1. The base iron (2.45 wt.% C, 30 wt.% Cr, 0.11 wt.% N) solidified as a near-eutectic alloy, indicating that in the real alloy the eutectic point is shifted towards lower carbon contents (about 2.45 wt.%) and a slightly lower eutectic transformation temperature T_E=1280.8°C compared to the values T_E=1288°C and C= 2.66 wt.% calculated for the ternary Fe–Cr–C system.
2. The investigated material is a fully ferritic high-chromium cast iron containing M_7C_3 carbides, no austenite or $M_{23}C_6$ was detected by XRD and SEM.
3. A 1.5 wt.% Ti addition to the alloy changed the crystallization from near-eutectic to hypereutectic with T_L=1280°C and the eutectic transformation temperature T_E=1272°C, whereas 1,07% Ti did not change the crystallization path.
4. With Ti addition, the area fraction of the carbide phase increased from approximately 20% to 29% and the carbide morphology changed form needle-like to compact hexagonal.
5. The cast iron containing 1.5 wt.% Ti exhibited the lowest abrasive wear in the Miller test (ASTM G75), achieving a 35% reduction in cumulative mass loss compared to the unmodified cast iron.
6. The Ti addition did not increase the microhardness of the matrix or the carbides; the mean values were lower by 38 HV and 89 HV, respectively, but these differences were not statistically significant (ANOVA, $p > 0.05$, $n = 3$)
7. The addition of Ti to cast iron containing a significant amount of nitrogen led to the formation of Ti(C,N) particles of an undetermined C/N ratio, which form colonies, in agreement with the observations reported in [3,12,13]; the impact toughness decreased from 10.7 to 5.2 J/cm² with increasing Ti content.

Proposed mechanisms:

8. N-rich Ti(C,N) most likely forms in the liquid bath above the liquidus and acts as a heterogeneous nucleation substrate for M_7C_3; this, rather than the carbon consumed by Ti, is proposed as the main reason for the hypereutectic solidification of Ti8, with a possible contribution of the higher Si content.
9. The tendency towards lower microhardness, if confirmed by a larger number of measurements, may be attributed to the combined effects of carbon and nitrogen binding by Ti(C,N), changes in the carbide chemistry and orientation, and the substrate effect in the refined carbides.
10. The improved abrasion resistance without an increase in microhardness is attributed to the higher volume fraction, refinement and better matrix support of the carbides and to the presence of hard Ti(C,N), which restrict micro-cutting and carbide pull-out.
11. The reduction in impact toughness is attributed mainly to Ti(C,N) clusters acting as crack initiation sites

The investigated nitrogen alloyed high chromium cast iron, characterized by an increased volume fraction of refined M_7C_3 carbides and dispersed Ti(C,N) particles, maintains good slurry abrasion resistance and can be regarded as a material bridging the gap between relatively soft ferritic high chromium cast irons and extremely hard martensitic high chromium grades. In this system, wear resistance depends primarily on the size, morphology and volume fraction of the carbide phase and Ti(C,N) particles rather than on the microhardness of the individual phases, which makes it a promising candidate for components that must combine improved abrasion resistance with acceptable machinability and moderate impact loading, provided that the Ti content is limited to avoid excessive clustering of Ti(C,N).

Acknowledgements

The research was co-funded by the 6th edition of the Applied Doctorate Program.

References

[1] Studnicki, A., Dojka, R., Gromczyk, M. & Kondracki, M. (2016). Influence of Titanium on crystallization and wear

resistance of high chromium cast iron. *Archives of Foundry Engineering*. 16(1), 117-123. DOI: 10.1515/afe-2016-0014.
[2] Huang, Z.F., Xing, J.D., Zhi, X.H. & Gao, Y.M. (2014). Effect of Ti addition on morphology and size of primary M7C3 type carbide in hypereutectic high chromium cast iron. *Materials Science and Technology*. 27(1), 426-430. DOI: 10.1179/026708309X12601952777666.
[3] Dojka, M. & Stawarz, M. (2020) Bifilm defects in Ti-inoculated chromium white cast iron. *Materials*. 13(14), 1-19. DOI: 10.3390/ma13143124.
[4] Zhi, X., Xing, J., Fu, H. & Gao, Y. (2008). Effect of titanium on the as-cast microstructure of hypereutectic high chromium cast iron. *Materials Characterization*. 59(9), 1221-1226. DOI: 10.1016/j.matchar.2007.10.010.
[5] Wu, X., Xing, J., Fu, H. & Zhi, X. (2007). Effect of titanium on the morphology of primary M7C3 carbides in hypereutectic high chromium white iron. *Materials Science and Engineering A*. 457(1-2), 180-105. DOI: 10.1016/j.msea.2006.12.006.
[6] Kim, W. Y., Jo, J. O., Chung, T. I., Kim, D. S., & Pak, J. J. (2007). Thermodynamics of titanium, nitrogen and TiN formation in liquid iron. *ISIJ International*. 47(8), 1082-1089. https://doi.org/10.2355/isijinternational.47.1082.
[7] Pak, J. J., Jeong, Y. S., Hong, I. K., Cha, W. Y., Kim, D. S., & Lee, Y. Y. (2005). Thermodynamics of TiN formation in Fe-Cr melts. *ISIJ international*, *45*(8), 1106-1111.
[8] Ding, H., Liu, S., Zhang, H., Guo, J. (2015). Improving impact toughness of a high chromium cast iron regarding joint additive of nitrogen and titanium. *Materials and Design*. 90, 958-968. http://dx.doi.org/10.1016/j.matdes.2015.11.055.
[9] Bramfit, B.L. (1970). The effect of carbide and nitride additions on the heterogeneous nucleation behavior of liquid iron. *Metallurgical Transactions*. 1, 1987-1995. https://doi.org/10.1007/BF02642799.
[10] Ovcharenko, G., Nikonova, R.M., Tereshkina, S.A. & Lubnin, A.N. (2023) Influence of nitrogen on chromium cast iron structure and properties. *Metallurgist*. 67(3-4), 452-461. DOI:10.1007/s11015-023-01531-2.
[11] Shen, L.R., Wang, K., Tie, J., Tong, H.H., Chen, Q.C., Tang, D.L., Fu, R.K.Y. & Chu P.K. (2005). Modification of high-chromium cast iron alloy by N and Ti ion implantation. *Surface & Coatings Technology.* 196, 349-352. DOI: 10.1016/j.surfcoat.2004.08.165.
[12] Dojka, M., Kondracki, M., Studnicki, A. & Dojka, R. (2018). Crystallization process of high chromium cast iron with the addition of Ti and Sr. *Archives of Foundry Engineering*. 18(2), 57-64. DOI: 10.24425/122503.
[13] Dojka, M., Dojka, R., Stawarz, M. & Studnicki, A. (2019). Influence of Ti and REE on Primary Crystallization and Wear Resistance of Chromium Cast Iron. *Journal of Materials Engineering and Performance*. 28, 4002-4011. https://doi.org/10.1007/s11665-019-04088-x.
[14] Bedolla-Jacuinde, A., Correa, R., Quezada, J.G. & Maldonado, C. (2005). Effect of titanium on the as-cast microstructure of a 16% chromium white iron. *Materials Science and Engineering A*. 398(1-2), 297-308. DOI: 10.1016/j.msea.2005.03.072.
[15] Chunga, R.J., Tanga, X., Li, D.Y., Hinckley, B. & Dolman, K. (2009). Effects of titanium addition on microstructure and wear resistance of hypereutectic high chromium cast iron Fe–25wt.%Cr–4wt.%C. *Wear*. 267(1-4), 356-361. DOI: 10.1016/j.wear.2008.12.061.
[16] Liu, T., Sun, J., Xiao, Z., He, J. Shi, W. & Cui, C. (2023). Effect of multi-element microalloying on the structure and properties of high chromium cast iron. *Materials*. 16(9), 3292, 1-12. https://doi.org/10.3390/ma16093292.
[17] Gong, L., Fu, H., Yang, P., Ji, X., Yin, W. & Lin, J. (2023). Refinement of primary carbides and improvement of wear resistance of hypereutectic high chromium cast iron after modification. *Journal of Materials Research and Technology*. 24, 5724-5742. https://doi.org/10.1016/j.jmrt.2023.04.176.
[18] Wang, J., Xing, X., Zhou, Y., Qi, X. & Yang, Q. (2010). Refining effect of nitrogen on M7C3 carbides in hypereutectic Fe–25Cr–4C–0.5Ti–0.5Nb hardface coatings. *Materials Science and Technology*. 35(9), 1114-1122. DOI:10.1080/02670836.2019.1613060.
[19] Jo, J., Kim, W., Lee, C. & Pak, J. (2010). Thermodynamic Interaction between Chromium and Titanium in Liquid Fe–Cr Alloys Containing 30 mass% Cr. *ISIJ International*. 50(10), 1373-1379. https://doi.org/10.2355/isijinternational.50.1373.
[20] Pierson, H.O. (1996). *Handbook of Refractory Carbides and Nitrides: Properties, Characteristics, Processing and Applications*. Westwood, NJ: Noyes Publications. https://doi.org/10.1016/B978-081551392-6.50001-5.
[21] Wiengmoon, A., Chairuangsri, T., Brown, A., Brydson, R. Edmonds, D.V. & Pearce J.T.H. (2005). Microstructural and crystallographical study of carbides in 30wt.%Cr cast irons. *Acta Materialia*. 53(15), 4143-4154. DOI: 10.1016/j.actamat.2005.05.019.
[22] Liu, Q., Zhang, H., Wang, Q., Zhou, X., Jönsson, P.G. & Nakajima, K. (2012). Effect of cooling rate and Ti addition on the microstructure and mechanical properties in as-cast condition of hypereutectic high chromium cast irons. *ISIJ International*. 52(12), 2210-2219, https://doi.org/10.2355/isijinternational.52.2210.
[23] Tabrett, C.P., Sare, I.R. & Ghomashchi, M.R. (1996). Microstructure-property relationships in high chromium white iron alloys. *International Materials Reviews*. 41(2), 59-82. https://doi.org/10.1179/imr.1996.41.2.59.
[24] Zum Gahr, K.H. & Eldis, G.T. (1980). Abrasive wear of white cast irons. *Wear*. 64(1), 175-194. DOI: 10.1016/0043-1648(80)90101-5.
[25] Doğan, Ö.N. & Hawk J.A. (1995). Effect of carbide orientation on abrasion of high Cr white cast iron. *Wear*. 189(1-2), 136-142. DOI: 10.1016/0043-1648(95)06682-9.
[26] Doğan, Ö.N., Hawk, J.A. & Laird G. (1997). Solidification structure and abrasion resistance of high chromium white irons. *Metallurgical and Materials Transactions A*. 28, 1315-1328. https://doi.org/10.1007/s11661-997-0267-3.